Biomechanics

Introduction

Wheel-based locomotion for Mars applications has long been tested and their relative simplicity and superior energy efficiency; however, wheels lack the ability to adapt to rugged and abrasive terrains without compromising their explorative capabilities. Leg-based locomotion shows promise for higher versatility and obstacle negotiation. This paper aims to discuss the factors that impact the form and functionality of a Boston Dynamics robot - *Spot* - by addressing the differences in operating conditions across different planets from a biomechanical standpoint. By identifying these differences in scale, energetics, actuation, and performance, a more optimal configuration is proposed. As there are a multitude of considerations, this report focuses on addressing potential modifications for each dimension ceteris paribus before a final recommendation was made.

1 Problem Statement

Key planetary differences that affect the functionality of a biomechanical vehicle can be summarized in Table 1 [1].

Table 1: Environmental differences between planets

Environmental Parameter	Earth	Mars
Surface Gravity (ms^{-2})	9.81	3.71
Atmospheric Pressure (mbar)	1013.25	<10
Temperature Range ($^{\circ}C$)	-145, +20	-80, +55
Daylight Cycle (h)	24.0	24.6
Solar Irradiance (Wm^{-2})	1,361	586.2

The lower gravity is the most significant environmental difference, reducing the compressive forces and affecting locomotion dynamics, as will be discussed throughout. The lower atmospheric density leads to negligible shear and drag forces on the limbs. To illustrate, the shear force exerted by wind can be calculated using dynamic pressure 1

$$P_s = \frac{1}{2}\rho_a v_{\max}^2 \tag{1}$$

where ρ_a is the respective atmospheric density and v the maximum wind speed. Despite Mars dust storm speeds being measured up to 30 ms^{-1}, the dynamic pressure applied is < 9 Pa. Comparatively, the same wind speed on Earth exerts a pressure of 460 Pa. As a result, the smaller attritional forces reduce the work required for locomotion. Other differences, such as temperature and irradiance, have more practical consequences relating to material selection; the lower solar irradiance imposes a constraint on the minimum cost of transport. Mars's terrain also poses complications by nature of its loose regolith composition, leading to poor friction with implications for traction and slipping.

Spot and *Atlas* are two innovations by Boston Dynamics, selected as the primary candidates for modification. *Atlas* is a bipedal humanoid robot, while *Spot* is a quadruped [2]. Though neither robot was designed specifically for Mars, suitability can be evaluated by considering the advantages and disadvantages of each posture.

Due to a combination of lower gravitational effects and terrain irregularities, stability becomes a larger challenge and priority given the nature of autonomy required, making *Spot* a more viable candidate for modification. In quasi-static terms, an intuitive measure for the stability margin can be approximated as the distance from the center of mass projection to the closest edge of the convex hull defining the base of support. For *Spot* with an assumed uniform density, the margin is approximately 250mm compared to *Atlas*'s 69mm.

2 Structure

On Earth, the size of terrestrial animals is constrained by the square-cube law, leading to the scale of musculoskeletal systems having an upper limit to their characteristic length L [3]. From a purely structural perspective, mechanical failure occurs when compressive stresses due to weight - calculated using equation 2

$$\sigma = \frac{mg}{A} \approx \frac{\rho V g}{A} \qquad A \propto L^2 \tag{2}$$

in bones exceed their yield strength of $\sigma_y \approx 100$ MPa. As the characteristic length L can be shown to scale linearly with axial stresses σ, the largest terrestrial mammals are calculated to have a maximum characteristic length of 3 m
In the Martian environment, the lower gravity allows the limit assuming linear stress scaling to be extended for a characteristic length. Through dimensionality analysis, the theoretical upper bound for a legged vehicle is 9.2m , assuming its limbs mimic biological scaling trends. A lower bound can be estimated to ensure clearance for Mars operations. As maximum terrain incline is expected to be greater (up to $\theta = 30°$), this leads to a larger minimum height of 31.25 mm to ensure clearance.

For structural analysis, a static free-body diagram of *Spot* was made for the sagittal and coronal plane, used to demonstrate loading and stresses within the limbs as shown in Figure 1. Despite *Spot*'s design implying it belongs to a member of *canidae*, each of its limbs bears resemblance to the hind limbs of an *ungiligrade*, divided into two linkages - an upper femur and a lower tibia terminating in a rigid tarsal complex. Although this greatly simplifies the kinematics into a 2-degree of freedom system, the biomechanical trade-offs are discussed in section 4.

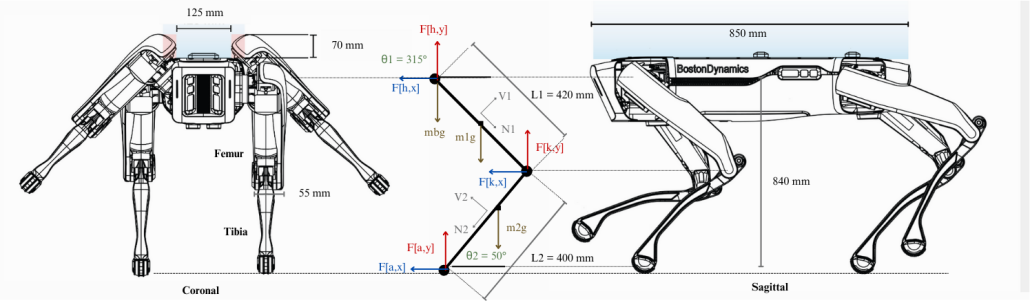

Figure 1: 2-DOF Free-body diagram of *Spot*

2.1 Limb Loads

Biological dimensions typically necessitate additional structural adaptations to maintain a safety margin to accommodate for dynamic loads. These include disproportionately thicker bones and shifts to posture [4]. On Earth, this non-uniform increase in characteristics relative to body size is known as allometry, which can be expressed via the relationship in 3

$$Y \propto X^{\alpha} \tag{3}$$

, where Y represents a dimension of interest, and X a size or mass variable. *Spot* weighs 35.2 kg with a femur length of 420 mm, which can be shown to align with empirical relationships found in *canidae* including $L \propto m^{0.33}$ and $A \propto m^{0.70}$. To analyze differences in internal loading to limbs, a system of equations for each linkage was derived as shown using the method of sections. Assuming the leg is in static equilibrium, with weight applied at the center of mass of each linkage and body weight acting through the hip joints;

$$N_1 = F_{h,x}\cos\theta_1 + F_{h,y}\sin\theta_1 - (m_b + m_1)g\sin\theta_1 \qquad N_2 = F_{k,x}\cos\theta_2 + F_{k,y}\sin\theta_2 - m_2 g\sin\theta_2 \tag{4}$$

$$V_1 = -F_{h,x}\sin\theta_1 + F_{h,y}\cos\theta_1 + (m_b + m_1)g\cos\theta_1 \qquad V_2 = -F_{k,x}\sin\theta_2 + F_{k,y}\cos\theta_2 + m_2 g\cos\theta_2 \tag{5}$$

$$M_1 = m_b g d_b + m_1 g d_1 \qquad M_2 = m_2 g d_2 \tag{6}$$

where N, V, M are the internal normal stresses, shear stresses, and bending moments for the femur (denoted with subscript 1), and tibia (subscript 2), or *Spot*'s frame (b) respectively. Reaction forces are notated at the hip joint, h, and knee joint, k, respectively, and decomposed into respective positive x and y Cartesian directions. d represents the perpendicular distances to weight vectors, with all θ angles measured from the vertical. Using continuum mechanics, the normal σ and shear stress τ components for each linkage are parameterized as:

$$\sigma_i = \frac{N_i}{A_i} + \frac{M_i y_i}{I_i}, \qquad \tau_i = \frac{V_i}{A_i} \tag{7}$$

As all gravitational terms enter equilibrium equations, each equation scales linearly with g. Thus, holding other parameters constant, internal axial and forces - along with normal and shear stresses - geometries can be up to 2.64 the scale of Earth before being strength limited, similar to the results from earlier.

This implies for Mars, optimal limb aspect ratios likely differ, with an ideal limb for performance having a higher aspect ratio to minimize weight and inertia to reduce the cost of locomotion. This is further discussed in section 3.
On the other end, a lower limit can be calculated by rearranging the Euler buckling criterion.

$$A_{\min} = \sqrt{\frac{12 m_{\text{eff}} g (KL)^2}{\pi^2 E}} \tag{8}$$

where A_{min} is the minimum cross-sectional area, g the gravitational acceleration, L the limb length, K the column effective length (set to 1 for pinned-pinned members), and E the Young's modulus. m_{eff} is the effective mass, which increases during dynamic movements by up to a magnitude of $2.0 - 2.9$ times [5]. Figure 2 illustrates this relationship between gravities, with an overlay of empirical *canidae* allometric scaling.

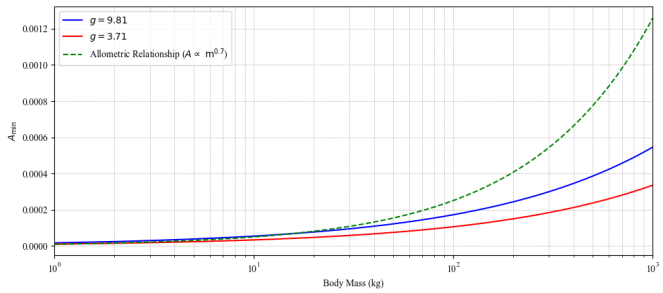

Figure 2: Minimum limb cross-sectional area relationship

Substituting available specifications from Spot, and estimating $E \approx 100$ GPa through averaging a combination of carbon-fiber and aluminum alloy compositions, a minimum cross-sectional area was calculated to be ~ 20.12 mm^2, roughly 61.5% smaller than ones on Earth. Through fundamental mechanics of materials, an absolute lower and upper bound can be placed for a limb possessing a configuration and aspect ratio to the Boston vehicle in both gravities. Here, L was kept at a constant to illustrate the discrepancy between allometric relationships and theoretical loading limits. In reality, varying limb length L will result in trade-offs against weight and idealized stride length. A modified *Spot* limb must also accommodate actuator attachments, joint articulations, and sensor interfaces, increasing the minimum practical cross-section beyond the results of purely buckling analysis.

2.2 Structural Design

Under normal gravity, higher ground reaction forces facilitate external stability, with a larger weight vector acting to counteract shifts in posture [6]. Under microgravity, the magnitude of reaction forces is reduced by the same proportion. As the proposed vehicle is designed with planned autonomy, modifications that improve stability are highly prioritized. The static stability factor is defined in Equation 9

$$\text{SSF} = \frac{\sqrt{Ag}}{2h} \tag{9}$$

where A is the base area, g is the gravitational acceleration and h the height of the center of gravity. In practice, a marginal $SST \geq 1$ is desirable to ensure stability.This implies that a *Spot* adapted for Mars should not exceed a characteristic ratio of $h_{\text{max}} = 0.963\sqrt{A}$ compared to $1.565\sqrt{A}$ on Earth.

As with limb internal stresses, bending moments due to the frame weight in both the coronal and sagittal plane scale linearly and thus are less strength-limited. Using *Spot*'s standard height of 840 mm, the dorsal plane is capable of accommodating up to 8.22 times the current area. Increasing additional dorsal capacity may be desirable for structural functions such as improved tipping resistance; a passive increase in lateral gait; but also ancillary functions including additional capacity for energy storage and generation without the typical drawbacks of higher wind shear loads on Earth.

2.3 Material

Robotic design faces other constraints due to the planet's low temperatures. With surface temperatures averaging to $-125°$C, aluminum and other metallic alloys experience a shift through the glass transition temperature. This can lead to a higher risk of brittle fracture during dynamic loading. Composites may encounter reduced interface bonding or matrix strength. Key considerations include ensuring a compatible coefficient of thermal expansion to minimize stress and incorporating active thermal management strategy - leading to increased passive energy consumption.

3 Energetics

Another perspective is through discussing the implications of the Martian gravity on the cost of locomotion and efficiency. For this, a rudimentary analysis was performed to illustrate the cost of a single walk cycle of *Spot*. Segment kinematics were extracted from a combination of inverse kinematics and positional information from video data, while anthropometric data was sourced from *Spot* specifications [2].

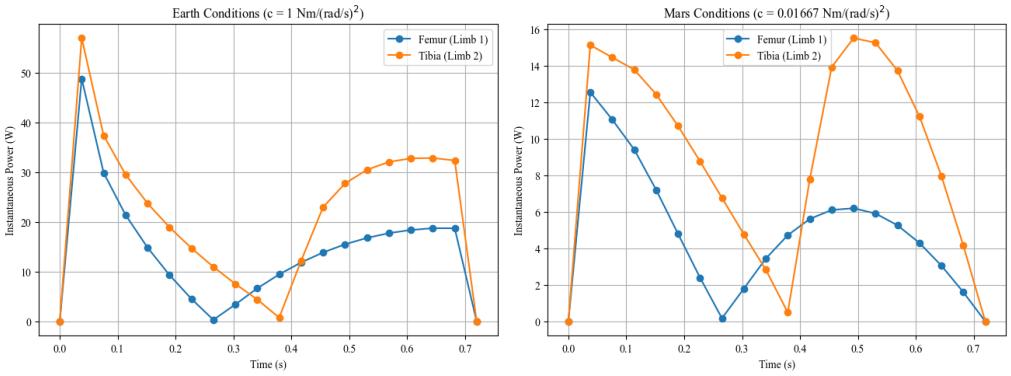

Figure 3: Internal mechanical work over a walk cycle for each limb

3.1 Cost of Locomotion

Cost of Locomotion is the mechanical work required, measured over a given stride, often standardized to a distance, and can be decomposed into internal and external components.

Internal work is defined as the mechanical energy due to relative movement, typically against the center of mass. While König's Theorem [7] is typically applied to partition a vehicle's individual linkages to represent the mechanical energy required as a sum of each segment' kinetic and potential energy contributions, it is limited by the assumption that all linkage velocities are identical under different conditions.

Instead, the resultant work required to move a segment was evaluated by addressing inertial and drag losses, expressed as a first-order differential equation;

$$I_{i,O}\frac{d\omega_i(\theta(t))}{dt} = T\theta - c\omega_i^2(\theta(t)), \qquad \omega_i^2(\theta(t)) = \frac{T}{c}\left(1 - e^{\frac{-2c\theta(t)}{I}}\right) \tag{10}$$

where $I_{i,\mathrm{CoM}}$ represents the moment of inertia of a segment i relative to the joint as it traverses through different angles taken from footage. The resultant angular acceleration, given by the derivative of ω, is calculated as the difference in the applied torque term, $(T\theta)$ against dissipative forces in the second term, parameterized by the drag coefficient c. Assuming a quadratic drag model and constant torque T, the net mechanical work for the combined 4 limbs on Earth is 37.92 J and 3.54 J on Mars.

External work refers to the work perturbations of the vehicle center of mass relative to the ground. While useful, the internal energy model is limited in its fixed height assumption, fixing the center of mass as a constant frame of reference for which the instantaneous energies of the swing phase are calculated. For an appropriate external work model, a different simplification was made. Using a central mass approximation [8] *Spot* in a walking gait can be simplified as an inverted pendulum concentrated at the center of mass. This constrains the mass to follow a simplified cosine trajectory as described in equation 11 within the sagittal plane, and considers the stance phase of movement as a sum of kinetic and potential energy components.

$$\Delta E_{\mathrm{external}}(t) = m_t g h_{\mathrm{CoM}}(t) + \frac{1}{2}m_t\left(L\frac{d\theta(t)}{dt}\right)^2, \qquad \begin{cases}\theta(t) = \theta_{\max}\cos\left(\frac{\pi t}{s}\right)\\ h_{\mathrm{CoM}}(t) = L(1-\cos\theta(t))\end{cases} \tag{11}$$

where m_t is the total mass of *Spot*, concentrated at an instantaneous height h_{CoM}, and L the effective maximum height. Over a stride measured to be $T \approx 0.72$ s, this results in Figure 4 as displayed below:

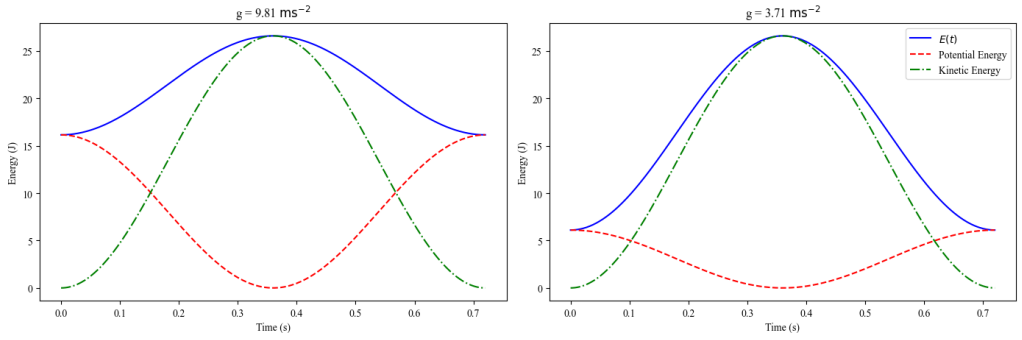

Figure 4: Instantaneous external work using the inverse-pendulum model

Work done was approximated by the summation of all instantaneous energy increments. Reconstructing joint angles and temporal data over each frame, the total mechanical work done was then calculated through summing instantaneous energy contributions in a single stride, given by Equation 12

$$W_{\text{mech}} = \int_0^T |\Delta E_{\text{external}}(t) + \sum_i^n \Delta E_{i,\text{internal}}(t)| dt \tag{12}$$

Total mechanical work on Mars was calculated to be $W_{\text{Earth}} = 37.92 + 17.49 = 55.21$ J, and $W_{\text{Mars}} = 3.54 + 6.66 = 10.20$ J on Mars.

For true cost of transport, all sources of metabolic outputs owing to locomotion must be considered. While mechanical work itself is derived in the section above, it neglects additional expenses in maintaining actuators for isometric force generation and stability throughout the stride cycle.

$$P_{\text{mech}} = \alpha F t + \frac{\dot{W}_{\text{mech}}}{\eta} \tag{13}$$

Equation 13 shows the metabolic power expenditure as partitioned between the instantaneous mechanical work component and continuous force generation. This term is comprised of a constant α determining the coefficient of actuation (~ 0.5 for pneumatic actuators), F to maintain a stance phase over the period t, and η the average muscle efficiency of metabolic to mechanical energy conversion - typically cited as 25%. As there is less effective weight, the isometric cost will inherently be lower. Using this, a robot with *Spot*'s dimension was estimated to draw ~ 421 W (with the actual robot rated at 400 W [2]), compared to an expected ~ 100 W on Mars.

3.2 Power Generation and Storage

Mars receives approximately 43% of Earth's solar irradiance with an average of 586.2 W/m^2, with a range of ± 137 W/m^2 due to orbital eccentricity. Additionally, frequent dust storms can deposit dust on exposed panels, reducing their efficiency and reliable generation of solar power.

Despite demonstrable success of advanced solar cells on the *InSight* lander reaching an efficiency of up to $\eta = 0.295$, conditions on Mars require improvements to locomotion efficiency especially in the transition towards legged-vehicles. To quantify the differences in power generation capabilities, the instantaneous power output per unit area was calculated. On Mars, P_{Mars} ranges between ~ 174 W/m^2 in clear conditions (59% of the theoretical maximum on Earth), to as low as ~ 10 W/m^2 in severe conditions. With *Spot*'s current dorsal area, a theoretical power threshold is ~ 9.74 W. Radioisotope generator technologies can exploit the additional dorsal capacity and low gravities to increase this threshold significantly with an additional 130 W.

Regarding electrical storage, significant temperature fluctuations and low temperatures can reduce the capacity and increase internal resistance of Lithium-ion batteries. Internal insulation for battery packs with active heating drawn from excess power may be considered to maintain optimal capacity; however, it may lead to increased weight and reduced vertical ground clearance.

3.3 Efficiency

The concept of locomotive efficiency as a ratio of output work and input during locomotion, is analogous to artificial vehicles. While *Spot* does not directly measure energy consumption aerobic glycolysis via oxygen volume metrics i.e. $\dot{V}O_2$ in the conventional sense, metabolic input can be defined as the theoretical baseline power calculated from the previous section, assumed as 130 W.

A percentage of this energy is allocated for maintenance in living organisms - processes that can be collectively referred to as the basal metabolic rate (BMR)[7]. The remainder of which can be allocated for locomotion, providing an estimate of metabolic efficiency η_m. The value of which may range between $0.3 - 0.4$ for most organisms, due to significant thermoregulatory, homeostasis, and biochemical demands. On the other hand, artificial vehicles have much lower continuous active demands, leading to potentially $\eta_m = 0.9$ of possible input power to be allocated to direct locomotion.

However, the higher efficiency is counterbalanced by when considering the thinner atmosphere present on Mars. Using the Nusselt number relationship for Newton's law of cooling in equation 14;

$$h \sim \frac{k}{L}\text{Nu}, \qquad \text{Nu} \sim \left(\frac{g\beta\Delta T L^3}{\nu^2}\frac{\nu}{\alpha}\right)^{0.25} \tag{14}$$

where k is the thermal conductivity of the atmosphere, L is the characteristic length of *Spot*. The Nusselt number is dimensionally similar to the quartic root of the product between the Grashof number and the Prandtl number. Terms include the thermal expansion coefficient (β)), temperature gradient (ΔT), kinematic viscosity (ν), and thermal diffusivity (α). Using typical conditions in Table 1 , convective heat transfer coefficient on Mars is approximately $h \approx 1.6$ W/m^{2}K, which is a factor of six lower than that on Earth. This implies a greater temperature difference is required for equivalent heat dissipation. To counteract this, active cooling systems may be required to ensure optimal operating temperatures - which are analogous to a form of BMR. Accounting for this, the effective metabolic efficiency is more likely closer to a value of $0.7-0.8$, leading to a maximum locomotive power threshold of ~ 100 W.

With calculated metabolic power using P_{mech}/η_m), *Spot* on Earth remains within 79% of total average metabolic input. In contrast, due to limited solar radiance, metabolic expense exceeds the threshold by 9% on average despite the lower cost of locomotion. This highlights a major constraint for designing vehicles for Mars.

4 Actuation

Actuation mechanisms in biomechanical robots can be broken down into three principal components - actuators, tendons, and joints. Actuators are components responsible for force and torque generation in response to an electrical stimulus, which mimic the role of biological muscles. Tendons transmit the generated force, routing it to different locations, and are additionally crucial for the efficiency of locomotion by the restoration of elastic energy. In human locomotion, up to $53-62\%$ of positive work is generated through this mechanism even under low speeds [9]. On Mars, the primary challenges stem from reduced gravitational loads, creating asymmetry in potential energy returns as shown in Figure 4. In reducing available compressive energy during the stance phase which can be transferred as mechanical work, vehicles designed on Mars must inherently be reliant on other means of energy conservation.

4.1 Elastic Restoration

The mechanism in which a muscle-tendon unit (MTU) stores and releases elastic energy can be generalized using a rudimentary Hill-type muscle model as displayed in Figure 5[7]

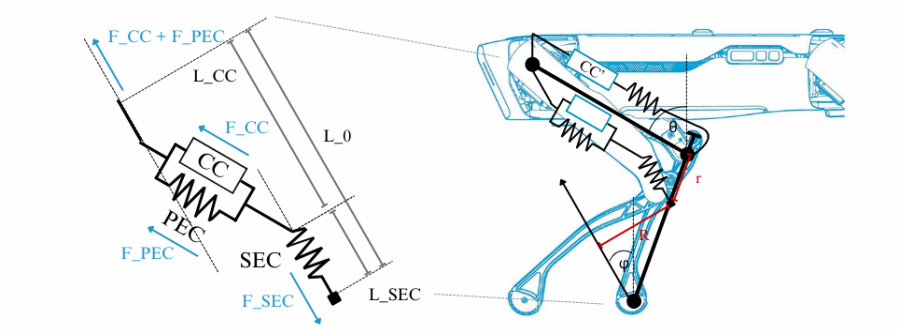

Figure 5: Simple Hill-type Muscle-tendon unit model on *Spot*

where *SEC* represents the series elastic components (tendons), *CC* the contractile components or active muscle fibers, and *PEC* representing the passive elastic properties. As the restoring force is reduced on Mars, several tendon properties may be varied to optimize the restoration force. These include the tendon stiffness (k_{SEC}) - which proportionally relates to the elastic energy stored - and slack length L_0.

Given the current 2 configuration of *Spot* in stance phase, the leg geometry can be incorporated into the calculation for optimal stiffness using inverse kinematics, such that the MTU strain between a fixed origin at the hip to an arbitrary position in the shank can be expressed as

$$\varepsilon_{\text{opt}} = \frac{L_{SEC} - L_0}{L_0}, \qquad L_0 = (L_{SEC} + L_{CC}) - L_{\text{opt}} \tag{15}$$

where ε_{opt} is the optimal tendon strain, derived from change in tendon length, L_{SEC}, slack length L_0 calculated from the MTU length and contribution of optimal tendon length. A nonlinear formulation for an artificial tendon-force length was used below[10]:

$$F_{SEC} = k_{SEC} L_0 \left(e^{\beta} \varepsilon_{SEC} - 1 \right) \tag{16}$$

where the β represents an arbitrary stiffness parameter. The Hill-type model states under isometric conditions, that all force generated by F_{CC} plus any passive contribution F_{PEC} must be in equilibrium within the tendon F_{SEC}, and equivalent

to the moment required about the joint M over its effective lever r. For optimal operating conditions, a constraint of $\varepsilon_{SEC} = \varepsilon_{\text{opt}}$ was imposed. Solving the system of equations in 15 , 16 via differentiation (i.e. $\frac{\partial F_{SE}}{\partial L_{SEC}}$ yields an expression for optimal tangent stiffness ;

$$k_{SEC,\text{opt}} = \frac{M(1+\varepsilon_{\text{opt}})}{r\varepsilon_{\text{opt}} L_0 \left(e^{\beta}\varepsilon_{opt} - 1\right)} \beta e^{\beta} \varepsilon_{\text{opt}}, \tag{17}$$

As shown, $k_{SEC,\text{opt}}$ is expected to decrease on Mars, implying that a more compliant tendon is more suitable for the lower compressive forces. Additionally, the term M is the moment generated by the actuator originating at the hip joint, directly affected by the tendon's insertion angle relative to the ground. On Mars, as only 37% of this moment is required for locomotion, a larger r - i.e. lower insertion point may be used to geometrically maximize the vertical component of the recoil force without mechanical constraints.

4.2 Mechanical Leverage

As direct elastic recovery of through purely spring mechanisms may not recover enough energy to be sufficient for sustained movements, modifications to mechanical leverage can be evaluated. Effective Mechanical Advantage (EMA) is the ratio of mechanical advantage r to the ground reaction force moment arm R, as referenced in Figure 5. In animals, EMA varies with individual muscle groups, sizes, and even speed. [11].

A similar linkage model to Figure1 was used to assess the impact of varying two parameters; shifting the tibia position relative to the joint, and the acute knee angle. From an equilibrium perspective, the minimum extensor actuator force required to counteract the gravitational torque acting on the knee joint can be shown as

$$F = \frac{mg(x\sin(\theta - \phi))}{d} \tag{18}$$

where m is the tibia mass, g the gravitational constant, d the tendon lever distance held constant, and x represents the effective moment arm, determined by the perpendicular distance between the knee joint and the tibia's center of mass. θ and ϕ define the acute angle subtended between links, and the normal component of the ground reaction force respectively. Thus, the EMA cost function can be derived as shown in equation 19.

$$EMA(x, \theta, \phi) = \frac{d}{x\sin(\theta - \phi)} \tag{19}$$

When both x and θ decrease, mechanical advantage increases, which is intuitive - a more extended knee angle and shorter effective tibia will geometrically increase the acting moment torque by an equivalent factor, regardless of gravitational conditions. In contrast, a higher ϕ is penalized (as only positive $\sin(\theta - \phi)$ values are structurally feasible), due to the magnitude of vertical reaction forces being reduced. While a lower ϕ may contribute to increased mechanical advantage, it should be noted that this creates a trade-off in stability. Recalling from section 2 that the static stability is derived through the size of the convex hull. A larger reaction force vector from the vertical results in the same deviation in the hip to compensate, increasing the size of the base projection.

4.3 Fast-Twitch Actuation

While these modifications improve passive energy recovery in the MTU, the lower reaction forces inherently constrain the additional energy that can be "multiplied". Even considering a tendon aligned geometrically to maximize the normal component, relying on momentum dynamics alone is likely insufficient to be mechanically sustainable.

Instead of conventional walking gaits, jumps and bounding gaits were explored, which biologically mimic predominant patterns in animals such as fleas and grasshoppers. These movements introduce additional force input by recruiting fast-twitch (type II) muscle fibers at the bi-articular antagonist muscle for the respective kinetic chain, as denoted by CC' in Figure 5. The leg-ankle extensors, the quadriceps group, represent the antagonist fibers to the Soleus/Gastrocnemius MTU complex. This locomotive strategy is typically characterized by an initially stretch-shortening cycle (SSC), which artificially loads the MTU, followed by a rapid concentric phase by the quadriceps. The contribution of SSC is marginal on Martian gravity, as previously discussed. While actuation of the quadriceps requires additional power, the generated torque is not affected by the gravitational acceleration and may be comparatively more efficient over long distances.

In the case of *Spot*, this actuator would originate along the posterior of the hip joint and insert below the knee. As this force generated is directly linked to the extension angle of the knee joint,

$$\tau(\theta) = F_m(\theta, \sigma, F_{\max}) \cdot r_{\max}\sin(\theta) \tag{20}$$

such that τ is the generated torque, $r_{\max}$ is the moment arm at maximum flexion , θ is the subtended knee angle, and F_m is the muscle force defined using a simplified Gaussian model and parameterized by the maximum force $F_{\max}$ and

its force-angle deviation σ. This allowed for a first-order approximation for quadriceps force output relationships as a function of extensor angle θ and the effective lever arm $L-x$.

$$F_{\text{ext}}(\theta,x) = \frac{F_{\max}}{L-x}\sin(\theta)\exp\left(-\frac{(\theta-\theta_{\text{opt}})^2}{2\sigma^2}\right), \qquad x < L \tag{21}$$

Equation 21 expresses the effective extensor force, F_{ext}.

A trade-off study for joint position was performed (Figure 6) against the parameters x and θ. $\alpha = 50^\circ$ was added to the θ in the F_{ext} expression to ensure both angle measurements followed the same position of reference. It is shown that a higher force production occurs at higher x, i.e. in configurations where the tibia is more distal, while the inverse is true for EMA; a closer tibia center of mass lends itself to a reduced relative inner lever arm. For θ, greater mechanical advantage is attained with larger deviations from the hip joint's passive stance angle of 45°. Optimal knee angle θ_{opt} defined the position of the "band" along the x-axis and arbitrarily set to 55°. In practice, CC' properties are typically adjustable for more optimal configurations.

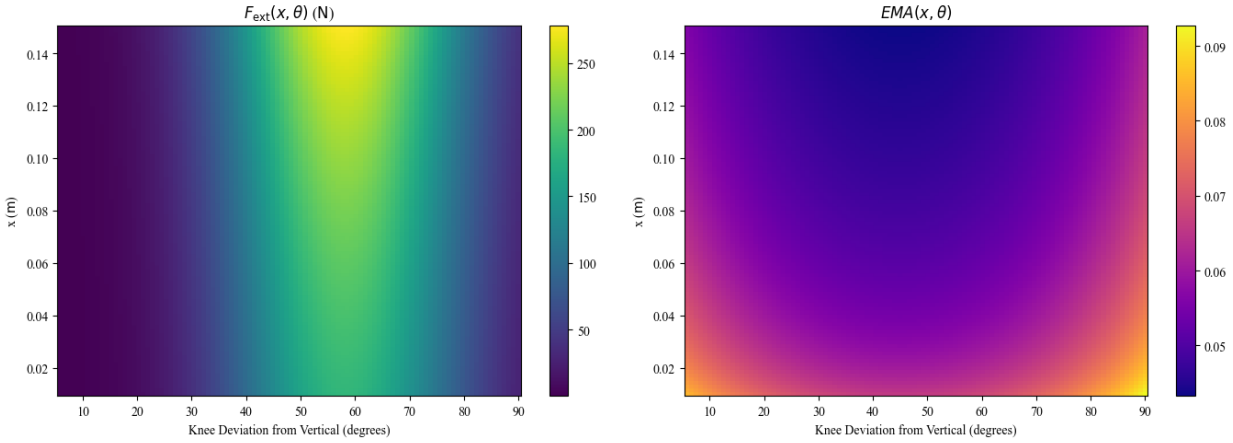

Figure 6: Propulsive force and Effective Mechanical Advantage tradeoff study

Force-velocity was neglected for the purposes of this analysis, as despite a clear interplay between contractile velocity and muscle force generation, it can be assumed that artificial fibers can be optimized for a suitable force-velocity profile [12].

4.4 Tarsal Modifications

Research shows that *unguligrade* locomotion, as found on *Spot* is generally more energy-efficient and suited for sustaining higher velocities for longer periods than animals which adopt *plantigrade* and *digitigrade* postures [13]. Despite this, it is important to note these comparisons only consider the operational efficiency over uniform terrains. In uneven surfaces such as Mars, the additional degree of freedom provided by the ankle joint found in the latter can reduce mechanical work expenditures by up to $10-15\%$.

It is found that the ankle joint can account for up to 89% of variation in limb work for non-steady locomotion [14], as the metatarsal is not fused and can conform dynamically, while also acting to distribute ground reaction forces over a larger surface area for improved traction on loose soil. Improved sensory granularity may be considered for adaptive terrain interaction, a mechanism which has been explored on other robots. An articulated ankle may improve the elastic energy recoil; an additional compliant element (akin to an Achilles tendon in humans) enables improved metatarsal alignment to maximize normal ground reaction forces, though this benefit may be marginal due to limited elastic recovery, as mentioned.

On the other hand, studies show the EMA of *digitigrades* typically reduces from $0.7-1.0$ to $0.3-0.6$, which may be a significant trade-off and demand reconsideration of scaling. Such modifications also add complexity via an additional degree of freedom, requiring more advanced control algorithms; with actuators in direct contact with abrasive terrain, which may pose challenges to durability in the context of remote missions. For such applications and the expected operational environment, the benefits of improved energy economy and terrain negotiation likely outweigh the sophistication of an added linkage.

5 Performance

Speed, acceleration, maneoveruability are all performance criteria for locomotor systems, and directly linked to power. While these are valuable metrics, this section discusses potential implications of assessing performance from independent factors.

5.1 Maximum Speed

Maximum speeds heavily depend on a multitude of factors. A simple analysis can consider dimensionality; for out-of-phase passive gaits such as walking, where potential and kinetic energy in the center of mass is cyclically exchanged, leading to a viable pendulum model in Figure 4. By dimensional analysis, this lends itself to the Froude number [7]:

$$\mathrm{Fr} = \frac{v^2}{gL} \tag{22}$$

where v is the walk velocity, g the gravitational acceleration constant, and L the characteristic length. In a simplified context, the maximum walking speed typically occurs at $\mathrm{Fr} \approx 0.5$. As such, the theoretical maximum walking speed on Mars is 1.24 ms^{-1}, or 61.5% compared to Earth.

The Froude number alone fails to capture the additional mechanical and energy contributions of MTUs which underpin running gaits, requiring a composite dimensionless index. Recent work shows that a combination of the physiological similarity index, Γ, which incorporates MTU limits as a ratio of the Borelli (Bo) and Hill (Hi) limits as shown in Equation 23[12].

$$\Gamma = \frac{\mathrm{Bo}^2}{\mathrm{Hi}^2} = \frac{(\varepsilon_{CC,\max} L)^2}{\frac{\sigma_{CC,\max}\varepsilon_{\mathrm{eff}}}{\rho_{MTU}}}, \qquad \varepsilon_{\mathrm{eff}} = \frac{1}{\beta}\left(\ln\left(\frac{m_{\mathrm{eff}} g}{k_{SEC} L}\right) + 1\right) \tag{23}$$

where $\dot{\varepsilon}_{CC,\max}$ is the maximum actuator strain rate (assumed to be 10 m^{-1}), $\sigma_{CC,\max}$ the maximum actuator stress, and ρ_{MTU} the unit density, and L the characteristic length, which are fixed for the purposes of comparison. m_{eff} is the effective dynamic mass supported by the unit - for a running gait at a given point, $\varepsilon_{\mathrm{eff}}$ is the effective SEC or tendon which can be derived from Equation 16, leading to a logarithmic relationship across different gravities. Substituting values and assuming fixed characteristics used on the current *Spot*,

$$v_{\max} = (gL \cdot \mathrm{Fr})^{\frac{1}{2}} \left(\frac{\Gamma}{1+\Gamma}\right)^{\frac{1}{2}} = \sqrt{gL}\sqrt{\frac{\dot{\varepsilon}^2_{\mathrm{CC,max}} L^2 \rho_{MTU}}{\frac{\sigma_{CC,\max}}{\beta}\left(\ln\left(\frac{m_{\mathrm{eff}} g}{k_{SEC} L}\right) + 1\right) + \dot{\varepsilon}^2_{\max} L^2 \rho_{MTU}}} \tag{24}$$

the theoretical maximum running velocity on Earth was predicted to be $v_{\max,E} = 1.68$ ms^{-1}, similar to speeds of what is found on similar quadruped robots such as *Spacebok*. The theoretical maximum on Mars under a runnning gait is $v_{\max,M} = 1.12$ ms^{-1} due to reduced effective strain and asymmetric gravitational recovery.

While maximum running velocity is a common metric of performance, it is likely less appropriate of a measure for Martian environments, especially as dimensionality analysis alone neglects to consider movement across varying terrain and different gaits.

5.2 Gait Optimisation

Across most terrestrial organisms, Taylor et al. explored the relationship between work and travel velocity, showing that the mechanical power varies linearly with speed. Naively, it can be inferred that slower speeds will consume more energy, leading to inefficiencies; however, this is not the case.

Animals adopt different gaits for different conditions. By altering the pattern of movement, locomotive efficiency can vary significantly with the gait of motion - as each movement pattern interplays with different energy-conservation mechanisms. On Earth, walking gaits cyclically balance the concentric and eccentric contractions to minimize energy expenditure. Due to an imbalance of these forces on Mars as referred to in section 3, there is a necessity to identify more conservative actuation patterns.

To assess the cost of transport, a numerical simulation was explored computationally on MATLAB. Explicit calculation of mechanical work done for each joint such as in equations 3.1 was attempted, but with a larger number of degrees of freedom and their derivatives, this was unsuccessful. Instead, a lower-order model was used; incorporating a double spring-loaded inverted pendulum (SLIP) model, with each spring unit representing the fore-limb and hind-limb complexes respectively [15]. Each gait pattern is characterized by alternating between different phases defined using the following

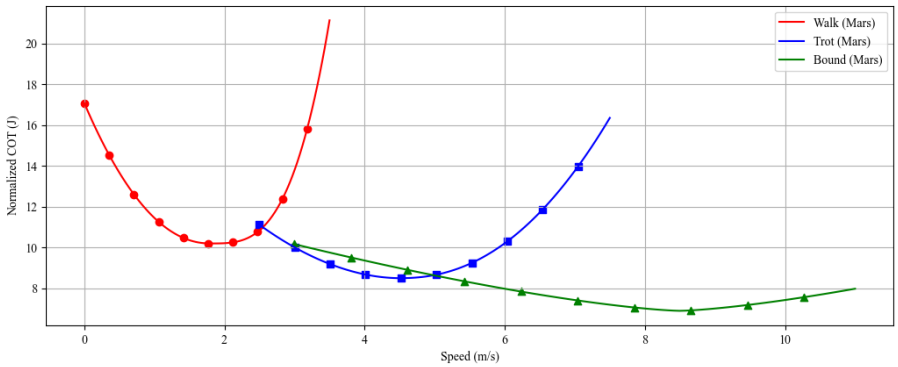

Figure 7: CoT per stride using SLIP model with exponential stiffness

system of equations. Cost of transport was calculated using an external work framework as in equation 4:
Flight phase (a_0):

$$\ddot{x} = 0 \ , \ \ddot{y} = -g \qquad\qquad \text{CoT} \approx 0 \tag{25}$$

Single stance phase (a_1):

$$\ddot{x} = \frac{k}{m}(l_0 - l(t))\hat{r}_x(t) \ , \ \ddot{y} = \frac{k}{m}(l_0 - l(t))\hat{r}_y(t) - g \qquad\qquad \text{CoT} = \frac{\eta k}{2\pi mgv}\sqrt{\frac{k}{m}}(l_0 - l(t)) \tag{26}$$

Double stance phase (a_2):

$$\ddot{x} = \frac{k}{m}(l_0 - l_1(t))\hat{r}_{x,1}(t) + \frac{k}{m}(l_0 - l_2(t))\hat{r}_{x,2}(t) \ , \ \ddot{y} = \frac{k}{m}(l_0 - l_2(t))\hat{r}_{y,1}(t) + \frac{k}{m}(l_0 - l_2(t))\hat{r}_{y,2}(t) - g \tag{27}$$

$$\text{CoT} = \frac{\eta k}{2\pi mgv}\sqrt{\frac{k}{m}}\sqrt{\frac{(l_0 - l(t))^2 - (l_0 - l_2(t))^2}{2}} \tag{28}$$

where $\hat{r}_i(t)$ denotes the instantaneous unit vector with respect to x, y Cartesian directions. For double stance phase, subscripts $1, 2$ denote the respective leg. k, l_0 and m denote the SLIP pendulum parameters, with CoT terms including η - the muscle conversion efficiency as taken from earlier- and v, the average forward velocity.

In walking, stances alternate between $[a_1, a_2]$. For trotting, a combination of both was used $[a_1, a_2, a_0]$, and $[a2, a_0]$ for bounding motions.

Figure 7 shows the CoT as simulated over walks while varying different forward velocities v. The results shows similar patterns to what is observed in literature. While it can still be shown that bounding gaits are more efficient on Mars with an optimal bounding gait of 6.901 ms^{-}1, without empirical data, it can only serve as an estimate. Other limitations include neglecting collision and damping losses, and assuming k_{SEC} is linear.

6 Conclusion

The report utilized a combination of taught models and methods, often in low-dimensional representations to illustrate differences for a specific aspect. While highly interpretable, low-dimensional representations often come at the cost of granularity and limitations for another, making the interplay in varying parameters less obvious. On Mars, design challenges often shift to stability and energy economy, redefining the concept of "performance" to ensure robust autonomy. Consequently, the optimal biomechanical parameters will be different to reflect the shift in the fitness function [7]. Often, multi-objective trade-offs must be performed between conflicting variables which necessitate computational methods.

Throughout the report, it was concluded that a modified *Spot* was allowed to be comparatively larger, with long and slender limbs with a higher aspect ratio while adopting a broader stance for stability. To ensure efficient locomotion, the vehicle would likely have a higher reliance on active input of energy from internal actuators as opposed to purely elastic energy recovery due to lower gravitational conditions. Its MTU components will require more compliant SECs, and an optimized force-velocity in the extensors. The knee joint should adjust to a more crouched stance to maximize mechanical advantage, with an added tarsal joint to be considered. *Spot* should preserve its limited power draw via adjusting to a more bounding gait pattern, or potentially a jumping pattern.

References

[1] J. Doe and J. Smith, Comparative analysis of earth and mars environments, *Planetary Science Journal* [online], vol. 10, no. 2 2023, pp. 123–135, 2023. DOI: 10.1234/psj.2023.045.

[2] Boston Dynamics, *Spot user guide, version r2.0*, 2020. available from: https://www.generationrobots.com/media/spot-boston-dynamics/spot-user-guide-r2.0-va.pdf.

[3] A. A. Biewener, Biomechanical consequences of scaling, *Journal of Experimental Biology* [online], vol. 208 2005, pp. 1665–1676, 2005. DOI: 10.1242/jeb.01520.

[4] R. M. Alexander, A. S. Jayes, G. M. O. Maloiy, and E. M. Wathuta, Allometry of the limb bones of mammals from shrews (sorex) to elephant (loxodonta), *Journal of Zoology, London* [online], vol. 189 1979, pp. 305–314, 1979. DOI: 10.1111/j.1469-7998.1979.tb03964.x.

[5] J. Nilsson and A. Thorstensson, Ground reaction forces at different speeds of human walking and running, *Acta Physiologica Scandinavica* [online], vol. 136, no. 2 1989, pp. 217–227, 1989. DOI: 10.1111/j.1748-1716.1989.tb08655.x. available from: https://pubmed.ncbi.nlm.nih.gov/2782094/.

[6] Ö. Drama, J. Vielemeyer, A. Badri-Spröwitz, and R. Müller, Postural stability in human running with step-down perturbations: An experimental and numerical study, *arXiv preprint arXiv:2004.02415* [online] 2020, 2020. available from: https://arxiv.org/abs/2004.02415.

[7] B. Department of Mechanical Engineering, *Energy: Mechanical energy in animal locomotion*, Discusses partitioning energy in biomechanics using König's theorem and the efficiency of locomotion, 2021.

[8] G. A. Cavagna, F. P. Saibene, and R. Margaria, Mechanical work in terrestrial locomotion: Two basic mechanisms for minimizing energy expenditure, *American Journal of Physiology* [online], vol. 233, no. 5 1976, R243–R261, 1976. DOI: 10.1152/ajpregu.1976.233.5.R243.

[9] A. K. M. Lai, G. A. Lichtwark, A. G. Schache, Y.-C. Lin, N. A. T. Brown, and M. G. Pandy, Tendon elastic strain energy in the human ankle plantar-flexors and its role with increased running speed, *Journal of Experimental Biology* [online], vol. 217, no. 17 2014, pp. 3159–3168, 2014. DOI: 10.1242/jeb.100826. available from: https://journals.biologists.com/jeb/article/217/17/3159/12443/Tendon-elastic-strain-energy-in-the-human-ankle.

[10] J. P. Charles, J. R. Baxter, K. D'Aout, and P. Aerts, Non-linear properties of the achilles tendon determine ankle stiffness during plantarflexion, *Journal of Experimental Biology* [online], vol. 226, no. 14 2023, jeb244863, 2023. DOI: 10.1242/jeb.244863. available from: https://www.ncbi.nlm.nih.gov/pmc/articles/PMC10399991/.

[11] A. A. Biewener, C. T. Farley, T. J. Roberts, and M. Temaner, Muscle mechanical advantage of human walking and running: Implications for energy cost, *Journal of Applied Physiology* [online], vol. 97, no. 6 2004, pp. 2266–2274, 2004. DOI: 10.1152/japplphysiol.00003.2004. available from: https://pubmed.ncbi.nlm.nih.gov/15258124/.

[12] D. Labonte, P. J. Bishop, T. J. M. Dick, and C. J. Clemente, Dynamic similarity and the peculiar allometry of maximum running speed, *Nature Communications* [online], vol. 15 2024, p. 2181, 2024. DOI: 10.1038/s41467-024-46269-w. available from: https://www.ncbi.nlm.nih.gov/pmc/articles/PMC10928110/.

[13] R. Kram and C. R. Taylor, Mechanical energetics of running: A comparison of humans with other mammals, *Journal of Experimental Biology* [online], vol. 193 1990, pp. 147–156, 1990. available from: https://spot.colorado.edu/~kram/bipeds.pdf.

[14] C. L. Dembia, A. Silder, T. K. Uchida, and S. L. Delp, Simulating ideal assistive devices to reduce the metabolic cost of walking with heavy loads, *PLoS ONE* [online], vol. 12, no. 7 2017, e0180320, 2017. DOI: 10.1371/journal.pone.0180320. available from: https://www.ncbi.nlm.nih.gov/pmc/articles/PMC6124028/.

[15] R. Blickhan, The spring-mass model for running and hopping, *Journal of Biomechanics* [online], vol. 22, no. 11-12 1989, pp. 1217–1227, 1989. DOI: 10.1016/0021-9290(89)90224-8.